Experiment and simulation of laminar and turbulent ferrofluid pipe flow in an oscillating magnetic field

Kristopher R. Schumacher and Inga Sellien*
Department of Chemical Engineering, University of Washington, Seattle, Washington 98195-1750

G. Stuart Knoke and Tahir Cader†
Energy International Inc., 127 Bellevue Way SE, Bellevue, Washington 98004-6229

Bruce A. Finlayson‡
Department of Chemical Engineering, Box 351750, University of Washington, Seattle, Washington 98195-1750
(Received 5 August 2002; revised manuscript received 18 October 2002; published 13 February 2003)

Laminar and turbulent pipe flow of a ferrofluid with an imposed linearly polarized, oscillating, magnetic field is examined here. Experimental results show a fractional pressure drop dependence on flow rate, magnetic field strength, and oscillation frequency. Calculations are presented, which show that ferrofluid theory can explain the flow phenomena in laminar and turbulent pipe flow. The model requires an initial fit of key parameters but then shows predictive capability in both laminar and turbulent flow. Simulation results are found to be essentially independent of the spin boundary condition due to an approximation of spin viscosity that is very small. A low Reynolds number k-ε model is used to model the turbulent pipe flow.

DOI: 10.1103/PhysRevE.67.026308 PACS number(s): 47.27.Eq, 47.15.−x, 47.27.−i

I. INTRODUCTION

A ferrofluid is a liquid with stable nanoscale magnetic particles suspended within it such that it responds strongly to magnetic fields. Brownian motion keeps the particles from settling in an external field, and an attached layer of surfactant helps prevent particle agglomeration. Applications such as hermetic seals in computer hard drives and increased heat transfer in electrical devices are possible due to the unique properties and behavior of ferrofluids.

In ferrofluid flows, the net effect of a magnetic field on the suspended nanoscale particles can be seen as an increase or decrease in the effective viscosity. This effect on effective viscosity has been the topic of a number of experimental studies and theoretical studies for Couette or Poiseuille flow. The current study is concerned with the effect of a linearly polarized, oscillating, magnetic field on pressure driven ferrofluid pipe flow in both laminar and turbulent flow regimes.

Some experimental studies of Poiseuille flow are available in the literature [1–4]. McTague [1] established that the effective viscosity increases with the application of a steady magnetic field and that the magnitude of this increase is dependant upon both the field strength and orientation. Bacri *et al.* [2] showed that when a linearly polarized magnetic field oscillates down the axis of the pipe at a high frequency, the effective ferrofluid viscosity can actually become lower than the viscosity in the absence of a magnetic field. The reduced viscosity, described for laminar flow by Bacri *et al.* [2] as $\mu_r(H,\Omega)=[\mu(H,\Omega)/\mu(0,0)]-1$, is referred to herein as the fractional pressure drop. Sometimes the literature refers to a negative viscosity effect, or sometimes even to a negative viscosity. Since the viscosity is always positive, and a reduction in viscosity is quite common with polymers where it is called shear thinning, the terminology ''negative viscosity effect'' is not used here. Further, Bacri *et al.* [2] showed how the fractional pressure drop depends upon the magnetic field strength and oscillation frequency and set the condition that the oscillation frequency Ω multiplied by the Brownian relaxation time τ_B must be greater than one for the fractional pressure drop to be negative. Zeuner, Richter, and Rehberg [3] conducted an experiment similar to Bacri *et al.* [2], with an ac solenoid wrapped around a portion of the pipe, but extended the study to a much larger range of magnetic field strengths and oscillation frequencies. The results of Zeuner, Richter, and Rehberg [3] also imply that $\Omega\tau_B \gtrsim 1$ when negative fractional pressure drops appear. Further, Zeuner, Richter, and Rehberg [3] present evidence that τ_B is a function of Ω. Table I compares the ranges of experimental conditions for both experiments. These experiments were limited to slow, laminar flows. Kamiyama [4] studied flow in a pipe with a dc solenoid creating a steady magnetic field. The data is limited to a single magnitude of the magnetic field, but does encompass both laminar and turbulent flow.

TABLE I. Comparison of the range of experimental conditions in Bacri, Perzynski, and Shliomis [2] and Zeuner, Richter, and Rehberg [3]. Brackets indicate powers of ten.

	Bacri *et al.* [2]	Zeuner *et al.* [3]
H range	0–1 Oe	0–500 Oe
Ω range	0–1 kHz	0–22 kHz
τ_B value	~1.6[−3] s	~9.4[−5] s

*Present address: DECHEMA e.V., Karl-Winnacker-Institut, Theodor-Heuss-Allee 25, 60486 Frankfurt am Main, Germany.
†Present address: Isothermal Systems Research, 511 3rd Street, Pullman, WA 99403.
‡Corresponding author.
Email address: finlayson@cheme.washington.edu

The results reported here are at an oscillation frequency range similar to Bacri *et al.* [2] (0–1 kHz), and at a field strength range larger than Zeuner, Richter, and Rehberg [3] (0–1264 Oe). Contrary to previous work, the results here are obtained for a range of laminar and turbulent flow rates in an oscillating magnetic field. The data show that the dependence of the fractional pressure drop on the flow rate is significant.

Theoretical studies of the flow of a ferrofluid with an applied magnetic field are also available in the literature [5–7]. Shliomis [5] used the equations of ferrohydrodynamics, a derived magnetization equation, and a nonlinear magnetic equation of state to study planar Couette flow with a constant magnetic field. His results compared well with the Poiseuille flow experiment of McTague [1]. More than 20 y later, Shliomis and Morozov [6] analyzed planar Couette flow with a linear polarized oscillating magnetic field. Using the same equations of ferrohydrodynamics and magnetization as Shliomis [5], they showed that the theory predicted that a negative fractional pressure drop could be achieved for any $\Omega\tau_B > 1$. While Bacri *et al.* [2] experimentally showed the existence of a negative fractional pressure drop, the predictions of Shliomis and Morozov [6] disagree with the behavior of the experimental data. Bacri *et al.* showed that the magnetization equation put forth by Marsenyuk, Raikher, and Shliomis [8] provided a truer prediction of the experimental data. Zahn and Pioch [9] investigated the torque felt by a ferrofluid particle in four different unsteady magnetic fields. Their analysis used the equations of ferrohydrodynamics, Shliomis' 1972 magnetization equation [5], and a magnetic equation of state with a constant effective magnetic susceptibility. Their use of a constant magnetic susceptibility allows them to develop an analytical solution to the nonlinear torque term in each of the four cases. Felderhof [7] studied Poiseuille flow in a pipe with a linear polarized oscillating magnetic field directed down the axis of the pipe. He used the equations of ferrohydrodynamics and considered three different magnetic relaxation equations, all with nonlinear magnetic equations of state. The three he investigated are: Shliomis [5], Martsenyuk, Raikher, and Shliomis [8], and Felderhof and Kroh [10]. His analysis concluded that the relaxation equation of Marsenyuk, Raikher, and Shliomis [8] provided a good estimation of the real behavior in a dilute ferrofluid, although they were all similar at small amplitudes of the oscillating magnetic field.

II. EXPERIMENT

The experiment is designed to study the laminar and turbulent fractional pressure drop of ferrofluid flow under the influence of a linearly polarized, oscillating, magnetic field. A schematic of the setup is given in Fig. 1. A peristaltic pump is used to pump the ferrofluid through the system at flowrates ranging from 330 $\mathrm{ml\,min^{-1}}$ to 1400 $\mathrm{ml\,min^{-1}}$. Pressure drop measurements are made over two equal length sections of 3 mm diameter pipe. Only one of the sections has an applied magnetic field. The fractional pressure drop is the pressure drop occurring in the section with magnetic field applied divided by the pressure drop occurring in the section without magnetic field minus one:

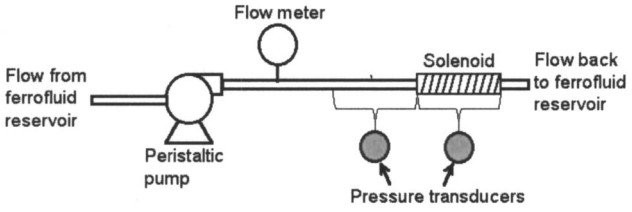

FIG. 1. Schematic of the experimental setup.

$$\frac{\Delta P(H)}{\Delta P(0)} - 1. \tag{1}$$

Thus, the increase in pressure drop due to this field is measured. Again, this fractional pressure drop in laminar flow is the same as the reduced viscosity mentioned in the literature.

Experimental results include pressure drop vs flow rate measurements at zero magnetic field and fractional pressure drop as it depends upon flow rate Q, magnetic field strength H_0, and frequency of oscillation of the magnetic field Ω. The experimental range of H_0 is 0–1264 Oe and the range of Ω is 0–1000 Hz. The experimental fluid is a water based ferrofluid, EMG-206, from Ferrotec.

Experimental results of the fractional pressure drop in the laminar and turbulent flow regimes as a function of H_0 and Q are shown for a Ω of 400 Hz in Fig. 2. The results show that in laminar flow the fractional pressure drop at a constant magnetic field decreases with increasing flow rate. Once the flow is turbulent, the fractional pressure drop is relatively constant for changing flowrates at a constant H_0. When the magnetic field strength is increased, the fractional pressure drop increases in all cases. These are the experimental results to be simulated.

In this experiment a negative fractional pressure drop is not observed. This does not contradict any results previously published; the experiment is just not in the range where this effect is expected. The previous experiments established that a general criterion for seeing a negative fractional pressure drop is $\Omega\tau_B \gtrsim 1$. The largest value estimated here is $\Omega\tau_B$

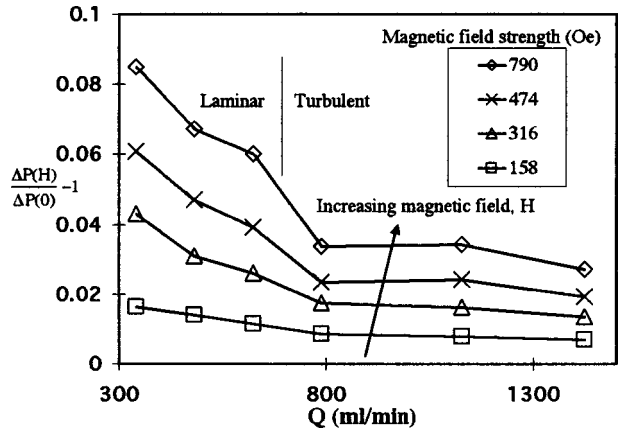

FIG. 2. Experimental fractional pressure drop as a function of the pipe flow rate and magnetic field strength at an oscillation frequency of 400 Hz.

$=0.061$. Our results agree qualitatively with the $\Omega\tau_B<1$ data of Bacri *et al.* [2] and Zeuner, Richter, and Rehberg [3].

The goal of this research is to use the equations of ferrohydrodynamics to predict and reproduce the experimental data from the pipe flow experiment in both the laminar and the turbulent regimes. This includes predicting the parameters that go into the governing equations, numerically solving the equations up to the boundary, and using a boundary condition on the particle spin that gives correct results. Numerical simulation of the ferrofluid flow allows us to deal with variable mean velocity and spin gradients.

III. MODEL EQUATIONS

The equations of ferrohydrodynamics as described by Rosensweig [11] are used to describe ferrofluid flow. They include an equation for linear momentum

$$\rho\left(\frac{\partial u}{\partial t}+u\cdot\nabla u\right)=-\nabla p+(\mu+\zeta)\nabla^2 u+2\zeta\nabla\times\omega+\mu_0 M\cdot\nabla H \tag{2}$$

and an equation for the spin rate (or internal angular momentum)

$$\rho I\left(\frac{\partial\omega}{\partial t}+u\cdot\nabla\omega\right)=\eta'\nabla^2\omega+2\zeta(\nabla\times u-2\omega)+\mu_0 M\times H, \tag{3}$$

where ρ is the density, μ is the dynamic viscosity, ζ is the vortex viscosity, μ_0 is the permeability of free space, I is the moment of inertia per unit mass of a ferrofluid particle, and η' is the spin viscosity. An equation for the magnetization M is also needed. The one proposed by Shliomis [5] is used here

$$\frac{\partial M}{\partial t}+u\cdot\nabla M=\omega\times M-\frac{1}{\tau}(M-M_0), \tag{4}$$

where M_0 is the equilibrium magnetization and τ is the relaxation time.

Simplifications to the momentum and spin equations are made to reduce them to a tractable form. First, steady, fully developed, axisymmetric flow in the pipe is assumed. Any entry and exit effects due to the oscillating magnetic field are ignored. Second, the magnetic field produced by the solenoid is assumed to vary only in time, making spatial gradients, i.e., the $M\cdot\nabla H$ term, equal to zero. Finally, the moment of inertia of a ferrofluid particle is so small that the convective term in the spin equation can be ignored. Using these assumptions and writing the equations in cylindrical coordinates gives

$$\frac{1}{r}\frac{d}{dr}r(\mu+\zeta)\frac{du}{dr}+2\zeta\frac{1}{r}\frac{d(\omega r)}{dr}-\left(\frac{\partial p}{\partial z}\right)_{\text{Constant}}=0 \tag{5}$$

and

$$\eta'\left(\frac{d^2\omega}{dr^2}+\frac{1}{r}\frac{d\omega}{dr}+\frac{\omega}{r^2}\right)+2\zeta\left(-\frac{du}{dr}-2\omega\right)+\mu_0 M\times H=0 \tag{6}$$

for the linear momentum and spin, respectively. The torque term in the spin equation is evaluated using the magnetization equation, following the work of Zahn and Pioch [9]. They assume a constant effective magnetic susceptibility, which allows for analytic expression of the torque. The convection term in magnetization equation (4) is zero for fully developed flow since the velocity and magnetization gradient are orthogonal. This is true in laminar flow and is assumed to be true in turbulent flow, too. The nondimensional torque term for a linear polarized magnetic field, time averaged over one period is

$$T_0\equiv\frac{\langle\mu_0 M\times H\rangle}{\mu_0 H_0^2}=\frac{0.5}{a^2+b^2}\chi_0[a(e-c)-\chi_0(ce+df)], \tag{7}$$

where

$$a=(\omega\tau)^2-(\Omega\tau)^2+1+\chi_0,$$

$$b=\Omega\tau(2+\chi_0),$$

$$c=\omega\tau+1,$$

$$d=f=\Omega\tau,$$

$$e=(1+\chi_0)-\omega\tau.$$

Equations (5) and (6) with Eq. (7) as the torque term are the set of equations that are solved for laminar flow.

For the turbulent flow, an additional assumption is made. Since the length scale of the ferrofluid particles is much less than the smallest length scale of the turbulence, the hypothesis is that the turbulence properties do not change from the case of a Newtonian fluid with the same viscosity as the ferrofluid. The Kolmogorov length scale ratio of largest eddies, L, to smallest eddies, η, is given as $L/\eta=\mathrm{Re}^{3/4}$ [12]. Dimensionally considering L to be the diameter of the pipe, 3 mm, and a Re of 10^4, the estimate for η is 3 μm, which is still much greater than the diameter of the particle, 30 nm.

In the turbulent flow analysis, the dependant variables are represented by a mean (represented by brackets, $\langle\rangle$) and fluctuating (represented by an asterisk,*) part, e.g., $u=\langle u\rangle+u^*$. Equations (2) and (3) are then time averaged. The time average of the turbulent spin equation remains the same as the laminar spin equation, assuming that the time average of the torque is the same as the time average over one period of oscillation. The time average of the momentum equation is not the same as the laminar case. Time averaging the nonlinear convective term introduces the closure problem; this means that there are now more unknowns than equations. The unknowns, called the Reynolds stress terms, have to be modeled. A two-equation eddy viscosity model is employed as a closure model to solve for the unknown Reynolds stress.

The time-averaged version of the momentum equation is given as

$$\frac{1}{r}\frac{d}{dr}\left[r\left((\mu+\zeta)\frac{d\langle u\rangle}{dr}-\langle u^*v^*\rangle\right)\right]+2\zeta\frac{1}{r}\frac{d(\langle\omega\rangle r)}{dr}-\left(\frac{\partial\langle p\rangle}{\partial z}\right)_{\text{Constant}}=0. \tag{8}$$

Using the eddy viscosity assumption, set the Reynolds shear stress component to

$$\langle u^*v^*\rangle=-\mu_T\frac{\partial\langle u\rangle}{\partial r}. \tag{9}$$

The bracket notation is dropped here and it is implied that all turbulent equations are now dealing with time-averaged quantities. The time-averaged momentum equation then becomes

$$\frac{1}{r}\frac{d}{dr}\left[r(\mu+\zeta+\mu_T)\frac{du}{dr}\right]+2\zeta\frac{1}{r}\frac{d(\omega r)}{dr}-\left(\frac{\partial p}{\partial z}\right)_{\text{Constant}}=0, \tag{10}$$

$$\text{where}\quad \mu_T=\rho C_\mu f_\mu\frac{k^2}{\varepsilon} \tag{11}$$

is the eddy viscosity. Now, two more equations are used for k, the turbulent kinetic energy, and ε, the turbulent kinetic energy dissipation rate. Specifically, the low Reynolds number k-ε model proposed by Myong and Kasagi [13] is used because, when it was developed, it was tested against fully developed pipe flow; thus, it directly relates to our situation. Further, the Myong and Kasagi model [13] was shown to give the best flow predictions in a pipe when compared to nine other models by Hrenya *et al.* [14]. The general form of the low Reynolds number k and ε equations for steady, fully developed, turbulent pipe flow are given [14] as

$$\frac{1}{r}\frac{d}{dr}r\left(\nu+\frac{\nu_T}{\sigma_k}\right)\frac{dk}{dr}+\nu_T\left(\frac{du}{dr}\right)^2-\varepsilon-D=0, \tag{12}$$

$$\frac{1}{r}\frac{d}{dr}r\left(\nu+\frac{\nu_T}{\sigma_\varepsilon}\right)\frac{d\varepsilon}{dr}+\frac{C_{\varepsilon1}f_1\nu_T\varepsilon}{k}\left(\frac{du}{dr}\right)^2-\frac{C_{\varepsilon2}f_2\varepsilon^2}{k}+E=0, \tag{13}$$

$$\text{where}\quad \nu_T=\frac{\mu_T}{\rho}.$$

By assumption, the effect of a vortex viscosity on the turbulent kinetic energy and rate of dissipation is neglected. The model constants, functions, and D and E terms depend on the specific low Reynolds number k-ε model being used. For the Myong and Kasagi model [13] they are

$$C_\mu=0.09,\quad C_{\varepsilon1}=1.4,\quad C_{\varepsilon2}=1.8,\quad \sigma_k=1.4,\quad \sigma_\varepsilon=1.3,$$

$$f_\mu=\left[1-\exp\left(-\frac{y^+}{70}\right)\right]\left(1+\frac{3.45}{\sqrt{R_T}}\right),$$

$$f_1=1, \tag{14}$$

$$f_2=\left[1-\frac{2}{9}\exp\left(-\left(\frac{R_T}{6}\right)^2\right)\right]\left[1-\exp\left(-\frac{y^+}{5}\right)\right]^2,$$

$$D=0,$$

$$E=0,$$

where $R_T=k^2/\nu\varepsilon$ and $y^+=[1-(r/R)]\mathrm{Re}_\tau$. The functions and constants in the Myong and Kasagi model [13] are not changed in our simulation.

Next, the laminar and turbulence equations are made nondimensional. In the laminar flow equations, the variables are normalized as follows: r by R, u by U_{AVG}, and ω by U_{AVG}/R. The normalized laminar equations are then

$$\frac{1}{r}\frac{\partial}{\partial r}r(1+C_1)\frac{\partial u}{\partial r}+2C_1\frac{1}{r}\frac{\partial(r\omega)}{\partial r}+C_2=0, \tag{15}$$

$$C_3\left(\frac{\partial^2\omega}{\partial r^2}+\frac{1}{r}\frac{\partial\omega}{\partial r}-\frac{\omega}{r^2}\right)+2\left(-\frac{\partial u}{\partial r}-2\omega\right)+C_4(T_0)=0. \tag{16}$$

For the turbulence equations r is normalized by R, u by u_τ, ω by u_τ/R, k by u_τ^2, and ε by u_τ^3/R. The normalized turbulent equations are then

$$2\,\mathrm{Re}_\tau+\frac{1}{r}\frac{\partial}{\partial r}r\left(1+\frac{\mu_T}{\mu}+C_1\right)\frac{\partial u}{\partial r}+2C_1\frac{1}{r}\frac{\partial(r\omega)}{\partial r}=0, \tag{17}$$

$$C_3\left(\frac{\partial^2\omega}{\partial r^2}+\frac{1}{r}\frac{\partial\omega}{\partial r}-\frac{\omega}{r^2}\right)+2\left(-\frac{\partial u}{\partial r}-2\omega\right)+C_4(T_0)=0, \tag{18}$$

$$\frac{1}{r}\frac{d}{dr}r\left(1+\frac{\nu_T}{\nu}\frac{1}{\sigma_k}\right)\frac{dk}{dr}+\frac{\nu_T}{\nu}\left(\frac{du}{dr}\right)^2-\varepsilon\,\mathrm{Re}_\tau-D\left(\frac{R^2}{\nu u_\tau^2}\right)=0, \tag{19}$$

$$\frac{1}{r}\frac{d}{dr}r\left(1+\frac{\nu_T}{\nu}\frac{1}{\sigma_\varepsilon}\right)\frac{d\varepsilon}{dr}+C_{\varepsilon1}f_1\frac{\nu_T}{\nu}\frac{\varepsilon}{k}\left(\frac{du}{dr}\right)^2-C_{\varepsilon2}f_2\frac{\varepsilon^2}{k}\mathrm{Re}_\tau+E\left(\frac{R^3}{u_\tau^3\nu}\right)=0, \tag{20}$$

for the momentum, spin, kinetic energy, and dissipation rate, respectively. In the above equations

$$C_1=\frac{\zeta}{\mu}, \tag{21}$$

$$C_2=-\frac{R^2}{\mu U_{\text{AVG}}}\left(\frac{\partial p}{\partial z}\right)_{\text{Constant}}, \tag{22}$$

$$C_3=\frac{\eta'}{R^2\zeta}, \tag{23}$$

$$C_4=\frac{\mu_0 H_0^2 R}{\zeta u_\tau}, \tag{24}$$

and

$$\mathrm{Re}_\tau=\frac{u_\tau R}{\nu}, \tag{25}$$

are unitless parameters that arise from the nondimensionalization. The friction velocity is defined as $u_\tau=\sqrt{\tau_{\mathrm{wall}}/\rho}$, where τ_{wall} is the shear stress at the wall. The first derivative of velocity, which is needed in the k and ε equations, is evaluated analytically at each grid point based on current values of k, ε, and ω.

IV. PARAMETERS AND BOUNDARY CONDITIONS

To solve the problem for our particular ferrofluid, the parameters μ, ρ, ζ, η', τ_B, and χ_0 along with the boundary conditions have to be specified.

The dynamic viscosity μ is estimated by the regression of laminar ΔP vs Q data in the absence of a magnetic field. A value of $\mu=0.003\,852\,1$ Pa s is found from this analysis. The value of the density is accurately determined with a PAAR DMA 45 digital density meter and is $\rho=1187.4\ \mathrm{kg\,m^{-3}}$. This technique makes density measurements based on the natural frequency change of a *U*-tube oscillator when loaded with different gases or liquids.

The vortex viscosity is estimated using $\zeta=1.5\mu\phi_h$ [11], where ϕ_h is the hydrodynamic volume fraction of the particles. The hydrodynamic volume fraction is estimated by using $\phi_m=M_{S,\mathrm{FF}}/M_{S,\mathrm{SOLID}}$, $\phi_m/\phi_s=0.74$, and $\phi_h/\phi_s=10$, where ϕ_m is the solid magnetic part of the volume fraction, ϕ_s is the total solids part of the volume fraction, $M_{S,\mathrm{FF}}$ is the saturation magnetization of the ferrofluid, $M_{S,\mathrm{SOLID}}$ is the saturation magnetization of the magnetic solids that make up the ferrofluid. These equations are based on the analysis for water based ferrofluids by Berkovsky, Medvedev, and Krakov [15]. With $M_{S,\mathrm{FF}}=11.94\ \mathrm{kA\,m^{-1}}$ and $M_{S,\mathrm{SOLID}}=478\ \mathrm{kA\,m^{-1}}$, this makes $\zeta/\mu=C_1=\frac{1}{2}$ for our ferrofluid.

The spin viscosity is estimated using kinetic molecular theory of an ideal gas and multiplied by 1000 to get an estimate for our liquid since liquid viscosities are typically 100–1000 times larger than gas viscosities. Bird, Stewart, and Lightfoot [16] derive the dynamic viscosity of an ideal gas from a molecular point of view using a linear momentum balance. Our approach is similar except we use internal angular momentum instead of linear momentum. The resulting expression for the spin viscosity is

$$\eta'=\frac{2}{3}\sqrt{mkT}\frac{1}{\pi^{3/2}D_P^2}I. \tag{26}$$

If the ferrofluid particle is considered as a two-layered sphere with different densities in each layer (see Fig. 3) the moment of inertia per unit mass I is then

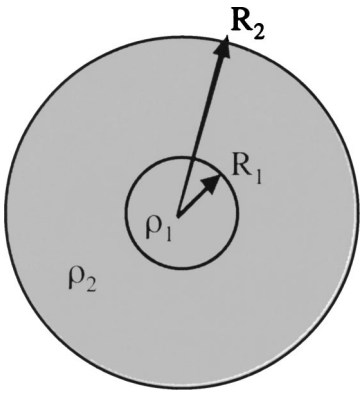

FIG. 3. A simple model of a ferrofluid particle is a two-layered sphere with different densities in each layer.

$$I=\frac{\frac{8}{15}\pi[\rho_1 R_1^5+\rho_2(R_2^5-R_1^5)]}{m}. \tag{27}$$

The spin viscosity estimate is a very small value of $6.4\times10^{-20}\ \mathrm{kg\,m\,s^{-1}}$ making $C_3=1.5\times10^{-11}$. Table II lists values of the parameters determined thus far.

The relaxation time physically relates to the amount of time it takes for a ferrofluid particle to orient its magnetization vector with an external field that is not originally in the same direction. Two types of relaxation times are relevant. The Brownian relaxation time refers to the actual rotation of the particle. The Néel relaxation time refers to the magnetization moment rotating inside of the particle. Brownian relaxation is typically much faster than Néel relaxation for particles with $D_P=10$ nm and larger; thus, the Néel component is ignored and the relaxation time τ is equal to the Brownian relaxation time τ_B. Shliomis [5] proposed that

$$\tau_B=\frac{3V_h\mu_c}{kT}, \tag{28}$$

where V_h is the particle's effective hydrodynamic volume, μ_c is the dynamic viscosity of the carrier fluid, and kT is thermal energy. Because the relaxation time is directly proportional to the volume of the particles, any agglomeration will lead to larger relaxation times. For turbulent flow this relaxation time is taken as a constant. For laminar flow, the relaxation time is allowed to vary with the flow rate and oscillation frequency. The hypothesis is that in turbulent flow the particle agglomerates will be broken up as far as pos-

TABLE II. Numerical values of selected parameters used in the ferrofluid model. Brackets indicate power of ten.

μ (Pa s)	3.85[−03]
ρ (kg m^{-3})	1187.4
ζ (Pa s)	1.93[−03]
η' (kg m s^{-1})	6.40[−20]
$C_1=\zeta/\mu$	0.5
$C_3=\eta'/R^2\zeta$	1.50[−11]

sible, giving a minimum relaxation time, but in laminar flow particle agglomerations can occur, especially since shear stresses go to zero at the center of the pipe. Specifically, we assume that particle agglomeration in laminar flow has a dependence upon shear rate and oscillation frequency. At lower flow rates, larger agglomerations are postulated to occur, causing τ_B to increase. Kamiyama [4] also suggests that the time constant in laminar flow is variable with flow rate, but is constant in turbulent flow. They relate this to agglomeration in their water-based ferrofluid. Zeuner, Richter, and Rehberg [3] also present evidence of a time constant dependence upon frequency.

Finally, the effective magnetic susceptibility is allowed to depend upon the strength of the magnetic field in different experiments, but a constant value is used at a given magnetic field strength. This is only an approximation, but it greatly simplifies the analysis. When a steady magnetic field is applied to our nonflowing ferrofluid and the resulting material magnetization is measured, the M vs H curve is nonlinear. At low field strengths the curve becomes almost linear (which means a linear magnetic equation of state is appropriate). The assumption is that the magnetic susceptibility in the case with flow and an oscillating H will exhibit the same basic behavior as can be found from an M vs H curve from a steady, nonflowing, case. That is, the magnitude of χ_0 decreases with increasing field strength.

To solve the laminar and turbulent equations, boundary conditions must be imposed for each of the dependant variables. The one-dimensional domain is from the center of the pipe $(r=0)$ to the wall of the pipe $(r=1)$. At the center of the pipe, the spin boundary condition is zero, $(\omega)_{r=0}=0$, while the other variables have the usual symmetry condition $(du/dr)_{r=0}=(dk/dr)_{r=0}=(d\varepsilon/dr)_{r=0}=0$. At the wall, the velocity fulfills the no-slip condition, $(u)_{r=1}=0$; the kinetic energy is equal to zero, $(k)_{r=1}=0$; the dissipation rate at the wall is $(\varepsilon)_{r=1}=(1/\mathrm{Re}_\tau)(d^2k/dr^2)$ [13]. The boundary condition for the spin rate at the wall is unknown but four different possibilities are evaluated: $(\omega)_{r=1}=0$, the spin is zero at the wall; $(d\omega/dr)|_{r=1}=0$, there is no couple stress at the wall; $(\omega)_{r=1}=\frac{1}{2}\boldsymbol{\nabla}\times u$ the spin of the particles is the same as that of a Newtonian fluid; and the ω equation is satisfied at the wall.

V. NUMERICAL METHOD

With boundary conditions and numerical values of the model parameters specified, the equations can be solved numerically. The laminar and turbulent equations are discretized and manipulated to ensure stability and positivity using the finite-volume method described by Patankar [17]. The laminar equations are also solved using the orthogonal collocation method [18] with only a few collocation points in the domain. Most simulations reported herein are derived using the finite volume method.

For each turbulent case, a mesh that increases its density as the wall is approached is used. This allows efficient and accurate resolution of profiles exhibiting steep gradients near the wall. The distance of the first node away from the wall is specified as $y_2=0.5/\mathrm{Re}_\tau$. As an example, turbulent flow at $\mathrm{Re}=5000$ with $N=40$ produces a $y_2=4.2\ \mu$m. With $R=1.5$ mm, y_2 is only 0.28% of the way to the center of the pipe. The benefit of using variable spaced nodes is apparent since 356 equidistant nodes (almost 9 times as many) are required to get the same y_2. For a given number of nodes N the rest of the mesh is generated using $y_i=y_{i-1}+(y_{i-1}-y_{i-2})P$, where P is the value that makes $y_N=1$. Note that $y_i=(r_i/R)-1$, and that the value of P, which is greater than 1, is found iteratively based on N.

The first derivative of velocity that appears in the spin, k, and ε equations is calculated exactly by integrating the momentum equation. This is possible because the pressure drop term is a constant. For example, doing this to Eq. (17) yields

$$\frac{du}{dr}=-\frac{(\mathrm{Re}_\tau r+2C_1\omega)}{\left(1+\dfrac{\mu_T}{\mu}+C_1\right)}.$$

This form of the derivative is then used in Eqs. (18)–(20). Doing this gives more stable solutions compared to when the derivative is approximated using a second order finite difference method.

The laminar and turbulent equations are discretized according to the finite-volume method. For each dependant variable $\mathbf{A}\varphi=\mathbf{b}$ has to be solved. The diffusion terms make $\mathbf{A}$ tridiagonal. Negative source terms are brought into $\mathbf{A}$ by the method of Patankar [17]. The unknown variable φ is solved for by lower-upper decomposition.

Because of nonlinear terms, iteration is necessary. Initial guesses for all variables are made. Then, the matrix equation for each dependant variable is updated separately. The order in which they are solved in is k, ε, ω, then u. The most current values of the dependant variables are always used in the terms that go into $\mathbf{A}$ and $\mathbf{b}$. The equations are iterated until the norm of the error,

$$\left\{\sum_{i=1}^{N}\left[(u_i^{\text{current}}-u_i^{\text{previous}})^2+(\omega_i^{\text{current}}-\omega_i^{\text{previous}})^2+(k_i^{\text{current}}-k_i^{\text{previous}})^2+(\varepsilon_i^{\text{current}}-\varepsilon_i^{\text{previous}})^2\right]\right\}^{1/2}, \quad (29)$$

at the current iteration is less than 1×10^{-6}

To solve at specified flowrates, the program is made to converge on a known value of the average velocity, $U_{\mathrm{AVG,specified}}$. This is accomplished by iterating about values of the nondimensional pressure drop using the secant method. The iteration continues until $|U_{\mathrm{AVG,simulated}}-U_{\mathrm{AVG,specified}}|<10^{-5}$.

The simulated pressure drop for the laminar flow is calculated using the Hagen-Poiseuille equation.

$$\frac{\Delta P}{L}=\frac{8\mu U_{\mathrm{AVG,simulated}}}{R^2}. \quad (30)$$

A force balance on the pipe using the value of stress at the wall is done to find the average pressure drop in turbulent flow,

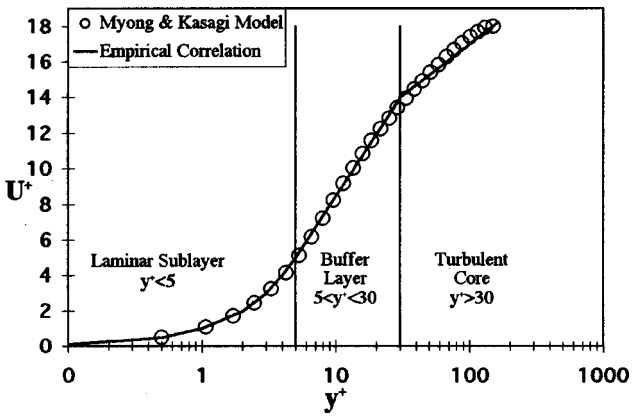

FIG. 4. The fully developed turbulent velocity profile for a nonmagnetic, Newtonian fluid compared to the empirical law-of-the-wall. The Myong and Kasagi k-ε model [12] with $\mathrm{Re}_\tau=150$. The empirical equations for the different layers are taken from Thompson [18]. U^+ is the velocity normalized by u_τ and y^+ is y normalized by ν/u_τ.

$$\frac{\Delta P}{L}=\frac{2\tau_w}{R}. \tag{31}$$

The stress at the wall, τ_w, is determined from the definitions of Re_τ and u_τ.

The fractional pressure drop in the turbulent simulations has an estimated error of 0.065% when 40 variable density grid points are used. The fractional pressure drop in the laminar simulations has an estimated error of 8.2×10^{-3}% when 30 equidistant grid points are used. Numerical accuracy is estimated by: finding the solution at various values of N, plotting the fractional pressure drop vs $(1/N)^2$, and extrapolating the fractional pressure drop to $(1/N)^2=0$ to get an estimate of the exact answer. Orthogonal collocation with from 3 to 7 collocation points gave results for the laminar flow that differed only by one in the ninth significant digit.

VI. RESULTS

This section is presented in three main parts: simulation of a nonmagnetic, Newtonian fluid flowing through a pipe, simulation of a ferrofluid flowing through a pipe with no magnetic field imposed, and simulation of ferrofluid flow through a pipe with a linear polarized magnetic field oscillating down the axis of the pipe.

A. Nonmagnetic, Newtonian fluid

The turbulent velocity profile for a nonmagnetic, Newtonian, fluid compares closely to the empirical law-of-the-wall (Fig. 4). The empirical equations for the different layers shown in Fig. 4 are taken from Thompson [19]. The friction factor also compares closely to the Blasius and Nikuradse equations at various turbulent Reynolds numbers. This gives confidence that the Myong-Kasagi low Reynolds number k-ε model [13] is being solved correctly.

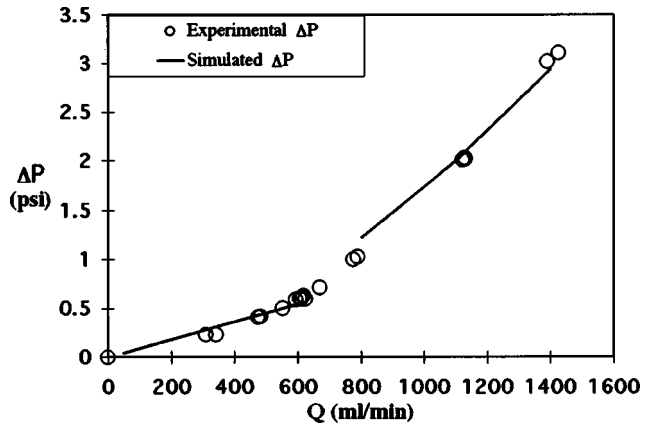

FIG. 5. Experimental ferrofluid pressure drop versus flow rate data, with the magnetic field turned off, compared to simulation. The model uses the parameters in Table II.

B. Ferrofluid, no magnetic field imposed

The ferrofluid model is used to simulate pressure drop versus flow rate data when the magnetic field is turned off. For both laminar and turbulent flow the values of the parameters in Table II along with $\tau=1.5$ μs and $\chi_0=0.04$ are used in the model. Again, the dynamic viscosity is obtained by a regression of the laminar $(H=0)$ data.

The results, in Fig. 5, are the same for all four boundary conditions of spin. In fact, the spin profiles for this case are identical except for a very thin boundary layer near the wall. Whatever the true boundary condition, the spin boundary layer here does not extend past the first node away from the wall. The reason is that the estimate of the spin diffusion coefficient η' is very small, removing the effect of the spin diffusion term. This observation holds in all subsequent simulations making the fractional pressure drop independent of the choice of spin boundary condition at the wall. The choice is made to use the boundary condition that satisfies the spin equation at the wall for all subsequent simulations. This boundary condition is chosen because it allows the spin profile to smoothly approach the wall. Others, namely, $(\omega)_{r=1}=0$ and $(\omega)_{r=1}=\frac{1}{2}\nabla\times u$, often displayed a dramatic visual discontinuity in the spin profile by jumping from the calculated value at y_2 to the value imposed at the wall. If the spin diffusion is completely neglected, the spin of a particle no longer depends on the spin rate of surrounding particles; it only depends on the torque induced by an external magnetic field

$$2\left(-\frac{\partial u}{\partial r}-2\omega\right)+C_4(T_0)=0. \tag{32}$$

C. Ferrofluid, linearly polarized, oscillating magnetic field imposed

Next, the problem is solved with the magnetic field turned on. The comparison of the simulated fractional pressure drop to experimental data over the range of experimental conditions is used to test the validity of the ferrofluid model.

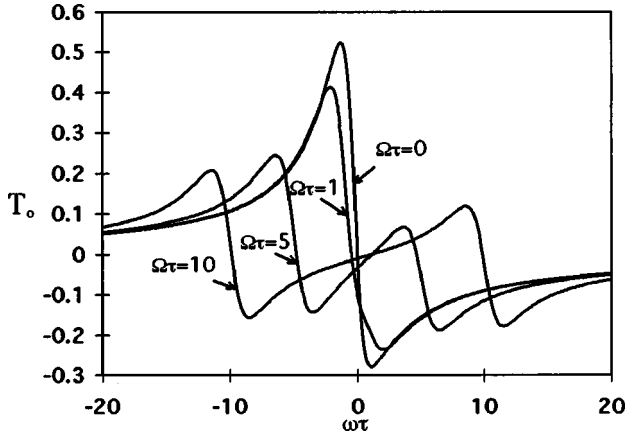

FIG. 6. Presentation of the nondimensional time-averaged torque term [Eq. (7)] for a linearly polarized magnetic field [8]. $\chi_0=1$. The products $\omega\tau$ and $\Omega\tau$ are also nondimensional.

In pipe flow, the vorticity is not constant, causing the spin to vary across the domain. As a result, there is a different value of the torque term at each discretization point in the domain (since the torque is dependent upon ω). Figure 6 shows the highly nonlinear behavior of the torque term as a function of spin and frequency derived from Eq. (7). The spin is zero at the center of the pipe, and at that point the torque in Fig. 6 is approximately zero for most simulations. The spin increases roughly linearly with radial position, so that the torque follows a line for constant Ω in Fig. 6. For small $\omega\tau$ (near the pipe center) this is linear, but for larger $\omega\tau$ (near the pipe wall at high flow rate) it is clearly nonlinear. Thus, the behavior in the pipe differs greatly with radial position, making the problem complex. The numerical results are found to be essentially independent of spin boundary condition because the magnitude of the spin viscosity removes the effect of spin diffusion, as was the case when there was no magnetic field.

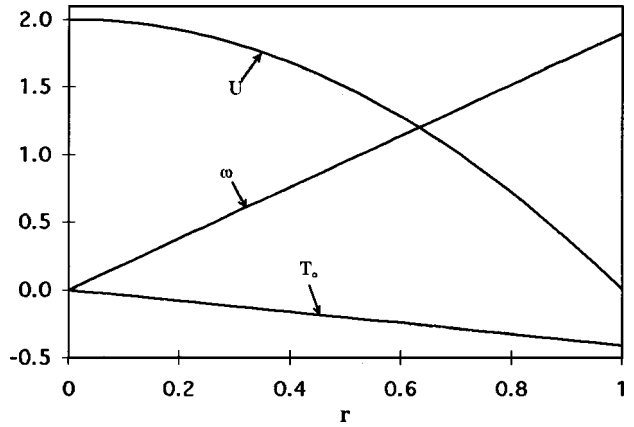

FIG. 7. Simulated profiles for laminar ferrofluid pipe flow with an imposed oscillating magnetic field. The nondimensional profiles are for: velocity, spin, and time-averaged torque. $Q=500\ \mathrm{ml\ min^{-1}}$; $H=948$ Oe; $\Omega=60$ Hz. The model parameters are as in Table II with $\tau_B=1.5\ \mu$s and $\chi_0=0.04$. U is normalized by U_{AVG}, ω by U_{AVG}/R, and torque by $\mu_0 H_0^2$.

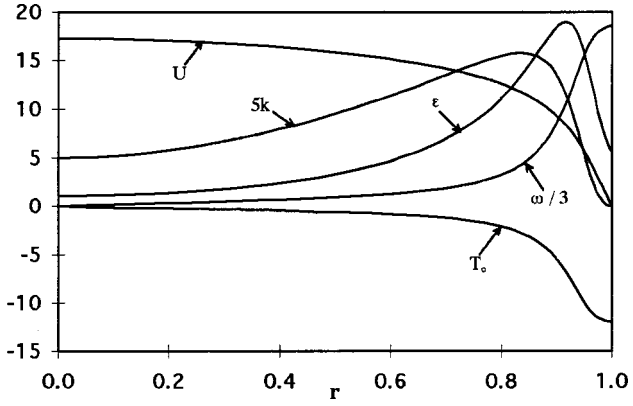

FIG. 8. Simulated profiles for turbulent ferrofluid flow with an imposed oscillating magnetic field. The nondimensional variables profiles are: velocity U, spin $\omega/3$, kinetic energy $5k$, dissipation rate ε, and time averaged torque T_0. $Q=1400\ \mathrm{ml\ min^{-1}}$; $H=948$ Oe; $\Omega=60$ Hz. The model parameters are as in Table II with $\tau_B=1.5\ \mu$s and $\chi_0=0.04$. U is normalized by u_τ, ω by u_τ/R, k by u_τ^2, ε by u_τ^3/R, and torque by $\mu_0 H_0^2$.

Profile results for laminar ($Q=500\ \mathrm{ml\ min^{-1}}$) and turbulent ($1400\ \mathrm{ml\ min^{-1}}$) flows with $H_0=948$ Oe, $\Omega=60$ Hz, $\tau=1.5\ \mu$s, $\chi_0=0.04$ and the parameters from Table II are shown in Figs. 7 and 8, respectively. The plots show the velocity, spin, and torque profiles, plus k and ε profiles for the turbulent simulation, plotted vs r. The torque appears to be linearly proportional to the spin; this is because τ is small enough to cause the quadratic terms in the torque equation, $(\Omega\tau)^2$ and $(\omega\tau)^2$, to become negligible. Figures 9 and 10 show how the laminar and turbulence variables shown in Figs. 7 and 8 change relative to the zero magnetic field case (with all other parameters the same). The solution profiles (excluding the torque) are normalized relative to their respective maximum value in the $H_0=0$ case. When the magnetic field is turned on, the laminar velocity profile does not visu-

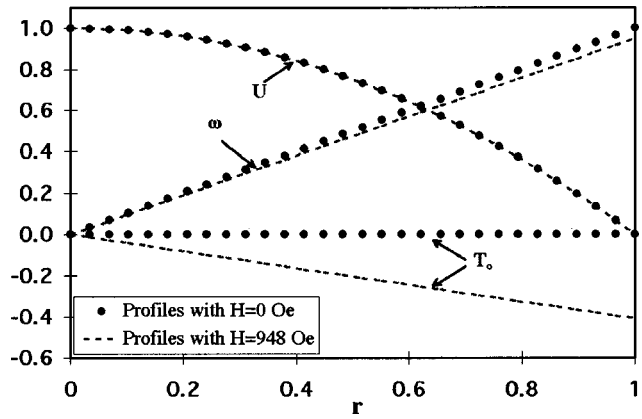

FIG. 9. Profiles from Fig. 7 as compared to the $H=0$ case. The velocity and spin profiles are normalized with respect to the maximum value of each corresponding dimensional variable in the $H=0$ case. The nondimensional, time averaged torque values are directly plotted, where the torque is normalized as in Fig. 7. The $H=0$ case is run using the same parameters as Fig. 7.

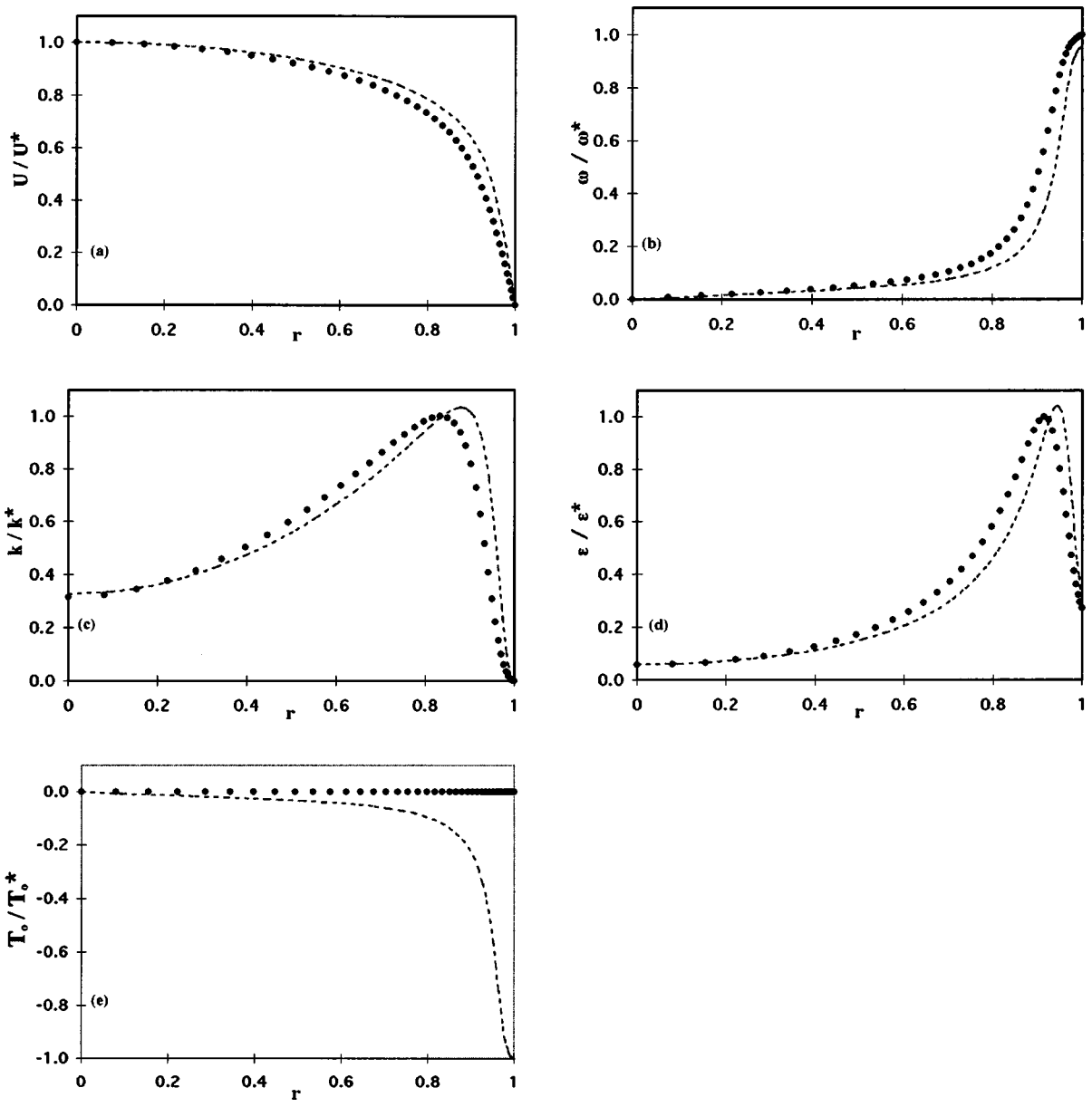

FIG. 10. Profiles from Fig. 8 as compared to the $H=0$ Oe case (a) velocity; (b) spin; (c) kinetic energy; (d) kinetic energy dissipation rate; (e) time-averaged torque. The dotted profile is the $H=0$ case. The dashed line is for $H=948$ Oe and $\Omega=60$ Hz. Plots (a)–(d) are normalized with respect to the maximum dimensional value in the respective $H=0$ case; $U^*=4.50\,\mathrm{m\,s^{-1}}$, $\omega^*=10179\,\mathrm{s^{-1}}$, $k^*=0.21\,\mathrm{m^2\,s^{-2}}$, $\varepsilon^*=216.3\,\mathrm{m^2\,s^{-3}}$. Plot (e) is normalized with respect to the negative minimum of the $H=948$ Oe case; $T_0^*=141.7$. The $H=0$ case is run using the same parameters as Fig. 8.

ally change but could be slightly different even though the flow rates are forced to be the same, but the laminar spin profile decreases because the torque impedes particle rotation. In the turbulent simulation the velocity profiles at the same flow rate are visually distinct. The spin profile decreases. The kinetic energy and dissipation rates increase and reach their peak values closer to the capillary wall.

One set of model parameters that fit all of the experimental data could not be found. However, by allowing two of the parameters to depend upon experimental conditions the model is able to reproduce and predict experimental data. Specifically, the effective magnetic susceptibility is allowed to depend upon magnetic field strength, and the Brownian time constant, in laminar flow only, is allowed to depend upon both flow rate and oscillation frequency. In all turbulent simulations the relaxation time is kept constant. The justification of allowing χ_0 and τ_B to depend upon experimental conditions is given in the ''parameters'' section.

In the turbulent simulations a value of the relaxation time has to be estimated, and we use the Eq. (26) proposed by Shliomis [5]. The time constant for the turbulent flow corresponding to a particle diameter of 29.5 nm is $\tau_B=9.8\,\mu$s. Using this value of τ_B, magnetic susceptibilities that make the model match the turbulent data are found at each field strength at 60 Hz and 800 $\mathrm{ml\,min^{-1}}$. The list of effective susceptibilities and corresponding field strengths are given in

TABLE III. List of magnetic susceptibilities and corresponding *H*.

H (Oe)	χ_0
158	0.0479
316	0.0278
474	0.0171
948	0.0063
1264	0.0043[a]

[a]Extrapolated value.

TABLE IV. List of relaxation times at corresponding Q and 60 Hz.

Q (ml min^{-1})	τ_B (μs)
342.7	61
482	41
624.2	36

TABLE V. List of relaxation times at corresponding Q and 400 Hz.

Q (ml min^{-1})	τ_B (μs)
341.5	29
482	24.5
624.2	20

TABLE VI. List of relaxation times at corresponding Q and 1000 Hz.

Q (ml min^{-1})	τ_B (μs)
311	24
475	18
611	13

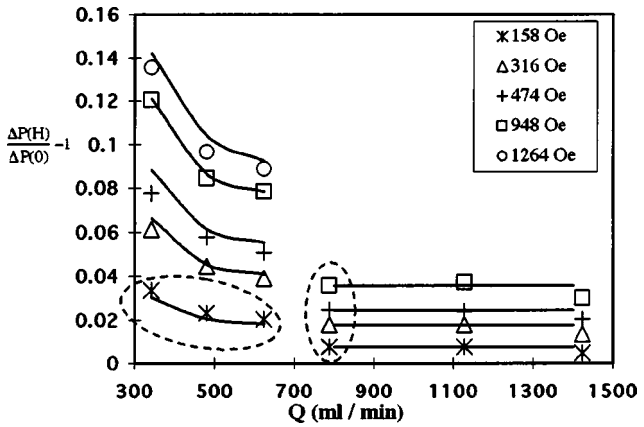

FIG. 11. Simulated fractional pressure drop results as a function of Q and H (represented with solid lines) compared to experimental data (represented with data points) at a constant frequency of 60 Hz. Note that a solid line is for a constant H value. Model parameters are as in Table II. Magnetic susceptibilities are as in Table III. Time constant values are as in Table IV. The data points within the dashed oval are used to determine parameters for this case.

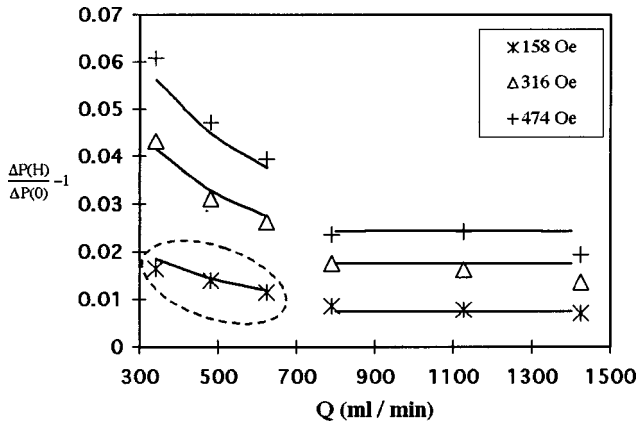

FIG. 12. Simulated fractional pressure drop results as a function of Q and H (represented with solid lines) compared to experimental data (represented with data points) at a constant frequency of 400 Hz. Note that a solid line is for a constant H value. Model parameters are as in Table II. Magnetic susceptibilities are as in Table III. Time constant values are as in Table V. The data points within the dashed oval are used to determine parameters for this case.

Table III. After this initial fit, when the frequency is raised (400 and 1000 Hz) the simulation predicts the turbulent data without having to adjust any parameters. Thus, all turbulent data (60, 400, and 1000 Hz) is predicted using our model with the parameters in Table II, a constant τ_B of 9.8 μs, and the magnetic susceptibilities in Table III.

The susceptibilities at a particular H for the laminar simulations are the same as those found to fit the turbulent data (see Table III). In laminar flow, the relaxation time is now allowed to depend upon flow rate and oscillating frequency. The list of laminar relaxation times and corresponding flow rates that fit the data at a field strength of 158 Oe and 60 Hz are given in Table IV. The list of relaxation times at 400 and 1000 Hz are given in Tables V and VI, respectively.

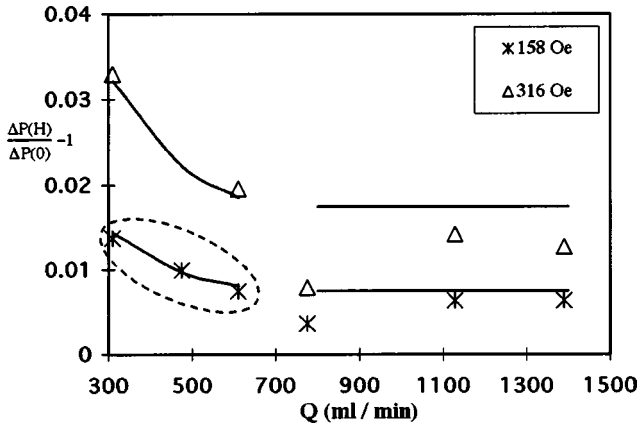

FIG. 13. Simulated fractional pressure drop results as a function of Q and H (represented with solid lines) compared to experimental data (represented with data points) at a constant frequency of 1000 Hz. Note that a solid line is for a constant H value. Model parameters are as in Table II. Magnetic susceptibilities are as in Table III. Time constant values are as in Table VI. The data points within the dashed oval are used to determine parameters for this case.

Figures 11–13 show laminar and turbulent fractional pressure drop results for 60, 400, and 1000 Hz, respectively. Experimental data are represented with data points; simulation results are represented by lines. The simulation results predict the laminar and turbulent experimental data reasonably well in all three figures.

In Fig. 11, the predictions for laminar flow and $H=316$, 474, and 948 Oe have no adjustable constants. The magnetic susceptibility is obtained from the turbulent data, but it does not exist for $H=1264$ Oe. Thus values of susceptibility, determined in the 60 Hz turbulence fit, are fit to a power formula, and then extrapolated to the higher magnetic field. The model gives slightly over predictive results when extended to $H=1264$ Oe in Fig. 11. Of the 27 data points shown in Fig. 11, only the 7 that are within the dashed ovals are used to determine the parameters; the other 20 data points can be predicted by the model. In Figs. 12 and 13 only 3 data points (within dashed ovals) are used to determine the parameters.

If the simulations use a value of τ_B four times larger than 9.8 μs, the simulation could only reproduce the data at 60 Hz (although not reported here). The data at higher frequencies could not be predicted because the large τ_B causes the quadratic terms in the torque equation to become more prevalent, and this limits the maximum fractional pressure drop we could calculate to values smaller than the data showed at high magnetic field and high frequency.

VII. CONCLUSIONS

Laminar and turbulent pipe flow with a linearly polarized magnetic field is studied experimentally and numerically. Experimental results show different behavior in laminar and turbulent flow regimes. A model based on the equations of ferrohydrodynamics [11] is used to predict the flow of ferrofluid in the unsteady magnetic field. The model accurately predicts the fractional pressure drop as a function of flow rate, magnetic field, and oscillation frequency, in both laminar and turbulent flow (as shown in Figs. 11–13) when the effective magnetic susceptibility is allowed to depend upon the magnitude of the magnetic field and the relaxation time (in laminar flow only) is a function of flow rate and frequency.

The spin viscosity is estimated to be so small that the spin diffusion is negligible. This makes simulation results effectively independent of the boundary condition of the spin. Our simulations suggest that spin profiles exhibit a very thin boundary layer next to the wall—only a few microns—and this is not resolved in these calculations. For our calculations, all spin boundary conditions give the same fractional pressure drop.

ACKNOWLEDGMENT

This research was supported by National Science Foundation Grant Nos. CTS-9908912 and DMI-9903582.

[1] J. P. McTague, J. Chem. Phys. **51**, 133 (1969).
[2] J. C. Bacri, R. Perzynski, M. I. Shliomis, and G. I. Burde, Phys. Rev. Lett. **75**, 2128 (1995).
[3] A. Zeuner, R. Richter, and I. Rehberg, Phys. Rev. E **58**, 6287 (1998).
[4] S. Kamiyama, *Magnetic Fluids and Applications Handbook*, edited by B. Berkovski (Begell House, New York, 1996), p. 475–487.
[5] M. I. Shliomis, Zh. Eksp. Teor. Fiz. **61**, 2411 (1972) [Sov. Phys. JETP **34**, 1291 (1972)].
[6] M. I. Shliomis and K. I. Morozov, Phys. Fluids **6**, 2855 (1994).
[7] B. U. Felderhof, Phys. Rev. E **64**, 021508 (2001).
[8] M. A. Marsenyuk, Y. L. Raikher, and M. I. Shliomis, Zh. Eksp. Teor. Fiz. **65**, 834 (1973) [Sov. Phys. JETP **38**, 413 (1974)].
[9] M. Zahn and L. L. Pioch, Ind. J. Eng. Mater. Sci. **5**, 400 (1998).
[10] B. U. Felderhof and H. J. Kroh, J. Chem. Phys. **110**, 7403 (1999).
[11] R. E. Rosensweig, *Ferrohydrodynamics* (Cambridge University Press, Cambridge, 1985/Dover, Mineola, N.Y., 1997).
[12] R. L. Panton, *Incompressible Flow* (Wiley, New York, 1996).
[13] H. K. Myong and N. Kasagi, JSME Int. J., Ser. II **33**, 63 (1990).
[14] C. M. Hrenya, E. J. Bolio, D. Chakrabarti, and J. L. Sinclair, Chem. Eng. Sci. **50**, 1923 (1995).
[15] B. M. Berkovsky, V. F. Medvedev, and M. S. Krakov, *Magnetic Fluids Engineering Applications* (Oxford University Press, Oxford, 1993).
[16] R. B. Bird, W. E. Stewart, and E. N. Lightfoot, *Transport Phenomena* (Wiley, New York, 1960).
[17] S. V. Patankar, *Numerical Heat Transfer and Fluid Flow* (McGraw-Hill, New York, 1980).
[18] B. A. Finlayson, *Nonlinear Analysis in Chemical Engineering* (McGraw-Hill, New York, 1980).
[19] W. J. Thompson, *Introduction to Transport Phenomena* (Prentice Hall, Upper Saddle River, NJ, 2000).